Low-Temperature Oxidation of Methane over Pd Supported on SnO_2-Based Oxides

Hardiyanto Widjaja, Koshi Sekizawa, and Koichi Eguchi*

Graduate School of Engineering Sciences, Kyushu University, 6-1 Kasugakoen, Kasuga, Fukuoka 816-8580

(Received July 23, 1998)

Pd catalysts supported on various metal oxides were investigated for the low-temperature catalytic combustion of methane. Of the catalysts examined, a Pd/SnO_2 catalyst demonstrated excellent activity despite its low specific surface area. The activity of the Pd/SnO_2 catalyst was lowered with the addition of M (= Al, Ce, Fe, Mn, Ni, and Zr) oxide to the support, Pd/SnO_2–MO_x. It was observed by a transmission electron-microscope observation that the PdO phase was well-dispersed on the outer surface of SnO_2 support uniformly, observed as an intimately contacted layer on fine SnO_2 particles. The temperature-programmed desorption of oxygen has revealed that the catalytic activity depends on the adsorption state of oxygen on palladium. An X-ray photoelectron spectroscopic analysis suggested that reduction of the palladium surface proceeded slowly under a strong palladium-support interaction for Pd/SnO_2. In situ X-ray diffraction indicated that the PdO phase was stabilized at higher temperature on SnO_2 than on the Al_2O_3 support. It is considered that the catalytic activity is strongly influenced by the interaction between palladium and SnO_2.

The catalytic combustion of hydrocarbons at high temperature, above 1000 °C, has been extensively investigated so far for the application to gas turbines, because of low thermal NO_x emission and high efficiency, as compared with conventional flame-combustion systems.[1,2] Although the operating condition of a combustor strongly depends on the catalyst activity and the air/fuel ratio, even a lean fuel mixture can be stably burned over a relatively wide range of temperature (400 to 1000 °C). For applications to low-temperature combustion, e.g., in direct drying of foods and polymers, the necessary heat can be supplied by the combustion of very lean mixtures over a highly active catalyst. Low-temperature catalytic combustion can also be applied for the cleaning of car exhaust, removing volatile organic compounds, flame-less heaters and household appliances operated below 1000 °C. These days, low-temperature combustion is also requested for the inlet zone combustor of gas turbines, aircraft afterburner, and other systems utilizing heat-radiation applications.[3]

Some noble metal catalysts have been known to be active for ignition reactions.[4] Palladium has been known to be the most active component for the combustion of methane. The morphological and chemical effects on the catalytic activity of Pd catalysts have been discussed, such as the dispersion of palladium particles, chemisorbed oxygen on Pd and surface reconstruction of palladium particles.[5—8] The nature of the interaction between oxygen and a Pd surface has been the subject of extensive studies in recent years. The development of Pd catalysts for methane oxidation should be based on understanding the reaction mechanisms in relation to oxygen–metal bonding. It has been known that the catalytic combustion of hydrocarbons on Pd catalysts proceeds by the reduction–oxidation cycle of Pd accompanied by the reversible adsorption and desorption of oxygen. According to our previous study, a high oxidation state of PdO is responsible for the high catalytic activity; the decomposition of PdO to metallic Pd gives rise to a drastic decrease in the coverage of the adsorbed oxygen leading to an inactive catalyst.[9] The correlation between the catalytic activity and the particle size of Pd has also been discussed.[7,10] Therefore, the dependence of the catalytic activity on the chemical state of palladium is quite complicated due to these entangled factors. It can be inferred that the performance of the catalyst is obviously related to the nature of the support through the dispersion of the Pd and Pd-support interaction.

Since sintering of metal particles results in simultaneous decreases of the active metal surface area and the activity, supported metal catalysts consisting of small metal crystallites dispersed on a support with a large surface area is widely used for all of the above-mentioned applications.[8,11] Alumina has been widely used as a support for the palladium catalyst due to its high specific surface area and low cost. The Pd/Al_2O_3 catalyst is active at medium temperatures above 400 °C to ensure complete combustion of methane to carbon dioxide and water. However, the activity of the Pd/Al_2O_3 catalyst is insufficient for low-temperature ignition, e.g., at 300 °C. Furthermore, the produced carbon dioxide and water serves as a poison for the Pd/Al_2O_3 catalysts, especially at low conversions and at low temperatures, making the activity deteriorated.[12]

In this study, the catalytic activities of palladium supported on various metal oxides were investigated for designing active ignition catalyst for methane combustion. The present study aims at examining the morphology of palladium on the support by transmission electron microscopy (TEM). Temperature-programmed-desorption of oxygen (TPD), X-ray

photoelectron spectroscopy (XPS), and in situ X-ray diffraction (XRD) were employed to evaluate the effect of the support on the redox properties of Pd species. The relation between catalytic activity and the morphological and the chemical properties of palladium particles was also discussed.

Experimental

1. Catalyst Preparation. Commercial metal oxide powders (MO_x; M = Al, In, Nb, Sn, Y, and Zr) were used as starting materials for oxide supports. These powders of oxides were calcined at 800 °C for 5 h in air. Mixed oxide supports (SnO_2–MO_x; M = Al, Ce, Fe, Mn, Ni, Zr) were prepared from aqueous $SnCl_4$ and metal nitrate solutions, and the composition of the solution was adjusted to the composition for a mixed oxide with molar ratio of $SnO_2/MO_x = 1$. The resultant precursor was dried and calcined at 800 °C for 5 h in air. Palladium catalysts were prepared by an incipient wetness technique using a palladium nitrate solution and the oxide powders. The loading of palladium in its metallic state was 1 wt% of the catalysts. The catalysts were dried and subsequently calcined in air at 800 °C for 5 h.

2. Catalytic Combustion of Methane. The activities of the catalysts for the combustion of methane were determined in a conventional flow reactor operating at atmospheric pressure. The catalyst (1 cm^3) was fixed in a quartz reactor by packing alumina beads at both ends of the catalyst bed. A gaseous mixture of methane (1 vol%) and air (99 vol%) was fed by a mass-flow controller to the catalyst bed at a flow rate of 48000 $cm^3\ h^{-1}$ (space velocity = 48000 h^{-1}). The effluent gas was analyzed using an on-line gas chromatograph (GC). A Porapak Q column was used for the separation of CH_4 and CO_2 and active carbon for the separation of CO. The catalytic activity was expressed by methane conversion calculated based on the following equation:

$$CH_4\ \text{conv.} = (1 - CH_{4\ out}/CH_{4\ in}) \times 100\%,$$

where $CH_{4\ out}$ is the flow rate of methane in the effluent gas and $CH_{4\ in}$ is the flow rate of methane in the feed gas before the reaction.

Crystalline phases and specific surface areas (Brunauer–Emmett–Teller (BET) surface area) of the catalysts were determined by XRD (Rigaku, RINT-1400) and by the BET method (Micromeritics, GEMINI-2370) using nitrogen as an adsorbate, respectively.

3. Transmission Electron Microscopy (TEM) Observation. A detailed investigation of the morphology of Pd particles impregnated on the support was carried out using a transmission electron microscope (TEM). For the TEM observation, a powder sample was dispersed in ethanol. A droplet of the suspension was put onto the sample holder with a microgrid using a pipet, and subsequently dried to make the TEM specimens. A JEOL JEM-2000FX electron microscope with an energy-dispersive X-ray analyzer (EDX, Tracor Nothern TN-2000) was employed, and a JEOL-4000EX electron microscope was used for high-resolution observations. The electron beam for the EDX analysis was focused to a spot with a diameter of ca. 20 nm.

4. Temperature-Programmed-Desorption (TPD) Measurement. The temperature-programmed-desorption (TPD) of oxygen was carried out in a flow system to observe oxygen desorption from catalysts. A standard reaction vessel was used for the TPD experiment.[13] A catalyst (1 g) was fixed in a quartz reactor by packing quartz wool at both ends. The length of the catalyst layer was 0.5—1.0 cm. Prior to the measurement, the sample was reduced in a He flow (50 ml min^{-1}) at 800 °C, followed by an O_2 flush (50 ml min^{-1}) at 800 °C for 2 h. After cooling in O_2 to room temperature, the feed gas was switched to a He stream (50 ml min^{-1}) for TPD. The sample was heated at a rate of 5 °C min^{-1} from room temperature to 800 °C, and the oxygen desorption was detected by using a thermal conductivity detector (TCD) cell and a mass spectrometer (ULVAC, MSQ-150A). A part of the outlet gas at ambient pressure was introduced to the differential high vacuum system, which was equipped with a mass spectrometer and a turbomolecular pump. It was confirmed that the readsorption of O_2 can be negligible due to the high He flow rate under this condition.[13]

5. X-Ray Photoelectron Spectroscopy (XPS) Measurement. To reveal the change in the electronic state of the supported Pd catalysts, XPS was employed. The X-ray photoelectron spectra were recorded at room temperature using a Shimadzu ESCA850 spectrometer with monochromated Mg $K\alpha$ excitation. Each sample was pressed into a pellet, clamped onto an XPS holder, and transferred into the XPS chamber. The background pressure in the spectrometer chamber was below 1×10^{-5} Pa.

Due to the charging effect of the supports, the core-level binding energy for oxidized palladium was often shifted toward a higher or lower binding energy (BE) on some support oxides. Consequently, the Au $4f_{7/2}$ (BE = 83.8 eV) signal was used as a reference to correct the XPS peak positions in all samples. Because of the strong overlap of the Au $4d_{5/2}$ and Pd $3d_{5/2}$ signals, the following procedure was employed. After measurements of Pd $3d_{5/2}$ and O 1s signals for the bare sample, Au particles were vacuum deposited. The binding-energy value of the O 1s signal was determined from the Au signal, and assumed to remain unchanged before and after Au deposition. Then, the binding-energy value of Pd $3d_{5/2}$ was determined with reference to the O 1s signal. Furthermore, due to the low concentration of palladium, 50 scans were accumulated in order to gain the signal-to-noise ratio. A Gauss-based fitting routine was used to peak fit the Pd core level spectra of Pd $3d_{5/2}$ and Pd $3d_{3/2}$.

6. In situ X-Ray Diffraction (XRD) Measurement. In situ XRD was employed for observing the crystalline phases of palladium species at high temperatures. Prior to the measurement, the sample was oxidized in an O_2 stream at 800 °C for 2 h followed by cooling to room temperature. Samples were then heated in a He flow at a heating rate of 20 °C min^{-1}, and kept at a given temperature for 15 min prior to the XRD measurement. In situ XRD patterns were recorded in a He atmosphere every 10—30 °C at between 700 and 900 °C.

Results

1. Oxidation Activity of Palladium Catalysts Supported on Various Metal Oxides. The catalytic activities for methane combustion over Pd catalysts supported on various oxides (MO_x; M = Al, In, Nb, Sn, Y, and Zr) are summarized in Fig. 1. In every case, carbon dioxide and water were the reaction products, but CO was not produced. The oxidation of methane over Pd/Al_2O_3 started at about 300 °C, followed by a steep increase in conversion up to 100% at 800 °C. The catalytic activity increased monotonously with rising temperature. The surface areas of the catalysts on other metal oxide supports were extremely low compared with that of Pd/Al_2O_3. The catalytic activities of Pd on In_2O_3, Nb_2O_5, and Y_2O_3 supports were very low. However, it is noted that Pd/ZrO_2 and Pd/SnO_2 catalysts exhibited a higher activity than did Pd/Al_2O_3 at all reac-

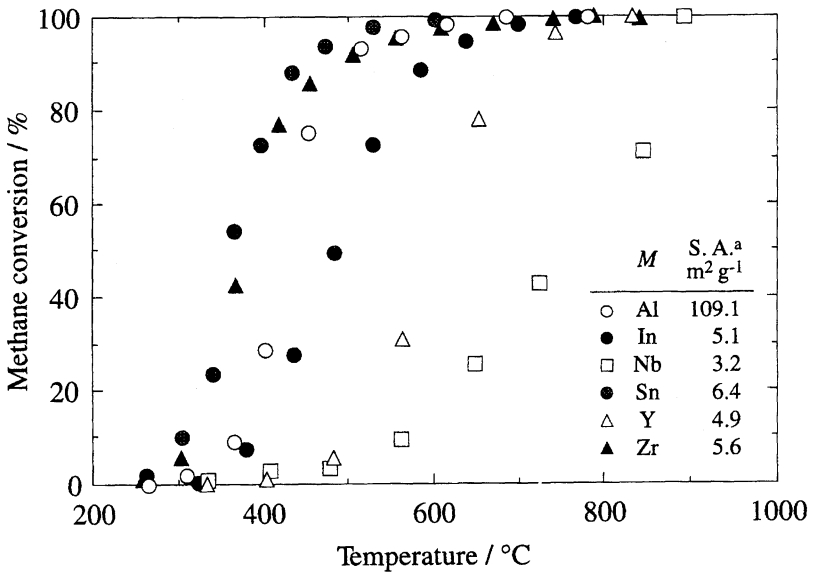

a) BET surface area.

Fig. 1. Catalytic combusion of methane over 1 wt% Pd/MO_x (M = Al, Ga, In, Nb, Sn, Y, and Zr). Reaciton conditions: CH_4, 1 vol%; air, 99 vol%; space velocity, 48000 h^{-1}.

tion temperatures. The sequence of the catalytic activities was M = Sn > Zr > Ag > In > Y > Nb. The activity curves shown in Fig. 1 were observed during the heating course of the catalyst, whereas the activity was sometimes lower than the values in the figure during the cooling course. This hysteresis was often observed for Pd/Al_2O_3, as some researchers have reported,[12] whereas the Pd/SnO_2 catalyst scarcely exhibited any activity difference between the heating and cooling courses. It is considered that, unlike Pd/Al_2O_3, the H_2O and CO_2 produced during the reaction have little influence on the activity of Pd/SnO_2. A high catalytic activity of Pd/SnO_2 was also observed for CO oxidation. Pd/SnO_2 and Pt/SnO_2 catalysts are known to be very active for CO oxidation because of a synergistic effect.[14—16] As a result, the reaction kinetics and the apparent activation energy of CO oxidation over Pd/SnO_2 catalyst is quite different from those over polycrystalline Pd, Pd/SiO_2, Pd/Al_2O_3, and SnO_2. However, the CH_4 oxidation characteristics of Pd/SnO_2 have not been satisfactorily reported. Among the catalysts given in Fig. 1, no simple correlation could be found between the activity and the BET surface area. Cullis and Willatt have also reported that the support has a pronounced effect on the rate of methane combustion over palladium catalysts.[8] Since Pd/SnO_2 exhibited the highest activity among the catalysts in the reaction temperature range investigated, the effect of additives to the Pd/SnO_2 catalyst was investigated in detail.

The catalytic activities and surface areas of Pd supported on various SnO_2-based oxides (Pd/SnO_2–MO_x; M = Al, Ce, Fe, Mn, Ni, and Zr) are summarized in Table 1. The overall activity of the catalysts was characterized by the temperatures at which methane conversion reaches 10, 30, 70, and 90%, as expressed by T10, T30, T70, and T90, respectively. The combustion of methane was significantly retarded by the presence of metal oxides incorporated in the SnO_2 support. The activity of a Pd/Al_2O_3 catalyst was sometimes enhanced

Table 1. Surface Area and Catalytic Activity of 1 wt% Pd/SnO_2–MO_x (M = Al, Ce, Fe, Mn, Ni, and Zr)[c]

Catalyst	Surface area[a]	Catalytic activity / °C			
	$m^2\ g^{-1}$	T10[b]	T30[b]	T70[b]	T90[b]
Pd/SnO_2	6.4	305	345	390	440
Pd/SnO_2–Al_2O_3	55.3	410	435	485	630
Pd/SnO_2–CeO_2	13.1	360	390	470	585
Pd/SnO_2–Fe_2O_3	1.8	435	515	675	825
Pd/SnO_2–MnO	1.4	500	595	760	855
Pd/SnO_2–NiO	4.0	425	440	470	540
Pd/SnO_2–ZrO_2	11.3	330	365	430	490

a) Calcined at 800 °C for 5 h. b) Temperature at which methane conversion levels are 10%, 30%, 70%, and 90%, respectively. Reaction condition: CH_4, 1 vol%; air, 99 vol%; space velocity, 48000 h^{-1}. c) Molar ratio of $SnO_2/MO_x = 1$.

by an additive to the support oxide.[17] In the case of Pd/SnO_2, the activity was hardly improved by the third component. Therefore, a further investigation was carried out only for Pd/SnO_2. No correlation could also be found between the catalytic activity and the BET surface area in this series of catalysts.

As we have reported previously, the Pd/Al_2O_3–NiO catalyst at a molar ratio of $Al_2O_3/NiO = 1/36$ and Pd loading of 1 wt% was very active for the oxidation of methane, as compared with Pd/Al_2O_3.[17] This active catalyst was subsequently expressed as Pd/Al_2O_3–36NiO. Therefore, Pd/Al_2O_3 and Pd/Al_2O_3–36NiO were employed as reference catalysts to evaluate the activity of Pd/SnO_2. As shown in Table 2, the catalytic activity of Pd/SnO_2 was at the same level as that of Pd/Al_2O_3–36NiO, except for a slight difference at a higher conversion region. The Pd/Al_2O_3, Pd/Al_2O_3–36NiO, and Pd/SnO_2 catalysts demonstrated significant differences in surface area. Although the BET surface area of Pd/Al_2O_3

Table 2. Surface Area and Catalytic Activity of 1 wt% Pd/Al_2O_3, 1 wt% Pd/Al_2O_3–36NiO,[c] and 1 wt% Pd/SnO_2

Catalyst	Surface area[a]	Catalytic activity / °C			
	$m^2\ g^{-1}$	T10[b]	T30[b]	T70[b]	T90[b]
Pd/Al_2O_3	109.1	365	400	445	495
Pd/Al_2O_3–36NiO	13.5	310	350	395	460
Pd/SnO_2	6.4	305	345	390	440

a) Calcined at 800 °C for 5 h. b) Temperature at which methane conversion levels are 10%, 30%, 70%, and 90%, respectively. Reaction condition: CH_4, 1 vol%; air, 99 vol%; space velocity, 48000 h^{-1}. c) Molar ratio of $Al_2O_3/NiO = 1/36$.

was the largest, this catalyst was less active than the other two catalysts. One important factor in enhancing the overall catalytic activity is to maintain the large active surface and/or fine microstructure of the palladium species. A large support surface is often necessary for attaining a high dispersion of Pd; however, for the present Pd catalysts, the catalytic activity may be influenced by the dispersion state of Pd species and its oxidation state rather than the gross BET surface area.[9,18—21] Some research groups have reported that the catalytic activity for methane combustion is independent of the dispersion of palladium particles,[8,22] whereas others have pointed out the influence of dispersion and the particle size of palladium.[4,5] It is therefore considered that a direct estimation of the particle size of palladium is important in explaining the rate of methane oxidation.

For the present Pd catalysts, the chemical interaction between the Pd particle and SnO_2 may strongly affect the dispersion. From our previous work, an X-ray line broadening analysis has been found to be effective in estimating the particle size of palladium.[17] However, in the case of Pd/SnO_2, experimental information concerning the Pd particle size could not be obtained from this method due to overlapping of the PdO (101) line with the SnO_2 (101) line.

2. TEM Observation. An observation of palladium particles by transmission electron microscopy (TEM) was employed in order to obtain direct information about their microstructure. A complete and reliable structural analysis of supported metal particles and their particle size is extremely difficult, even if the measurements are based on a careful statistical evaluation of electron micrographs. It is apparent that the observation of the Pd particles was generally too difficult due to the strong absorption and/or scattering of the incident beam by heavy Sn atoms. The large particle size of SnO_2, as indicated by the small BET surface area, is also an obstacle for TEM observations. As depicted in Fig. 2, it can be seen that most of the large particles are found to be SnO_2 particles for which Pd particles were hard to recognize, even if they were present. However, as indicated by the arrow, many fine particles of around 10—100 nm in size were also observed around the large particles, though their fraction was small. The fine particles observed in Fig. 2 were often produced by the disruption of large particles upon irradiation with an electron beam. Therefore, it is expected that a part

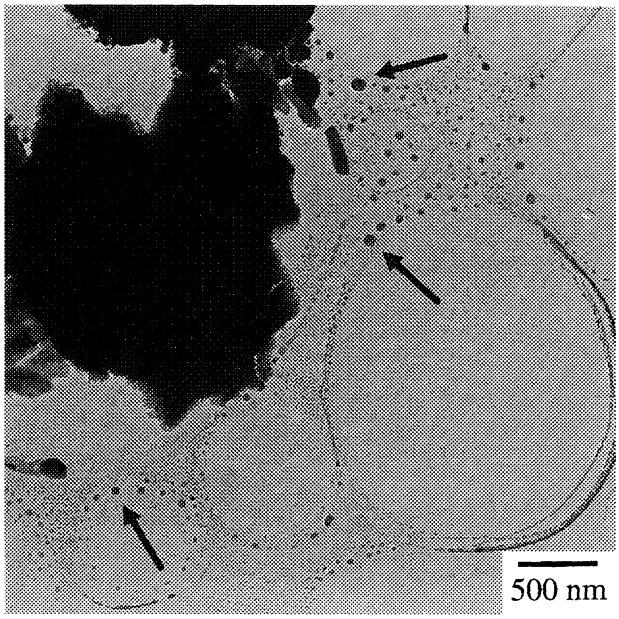

Fig. 2. High resolution TEM photograph of 1 wt% Pd/SnO_2.

of the large particles in Fig. 2 existed as an agglomerate of the fine particles. The fine particles were often observed in the surface region of large agglomerates.

From the EDX result shown in Fig. 3, it is evident that the fine particles consisted of Pd and Sn. It was difficult to estimate the composition of the large particle, since the detected X-ray did not give any average information from the particle. A microbeam electron-diffraction pattern of the fine particle showed only a [001] zone-axis pattern of the tetragonal SnO_2 structure (Fig. 4). It can be assumed that palladium particles were finely dispersed or poorly crystallized on the SnO_2 support.

To observe the atomic image of Pd/SnO_2, the high-resolution TEM of the fine particles was then employed. A

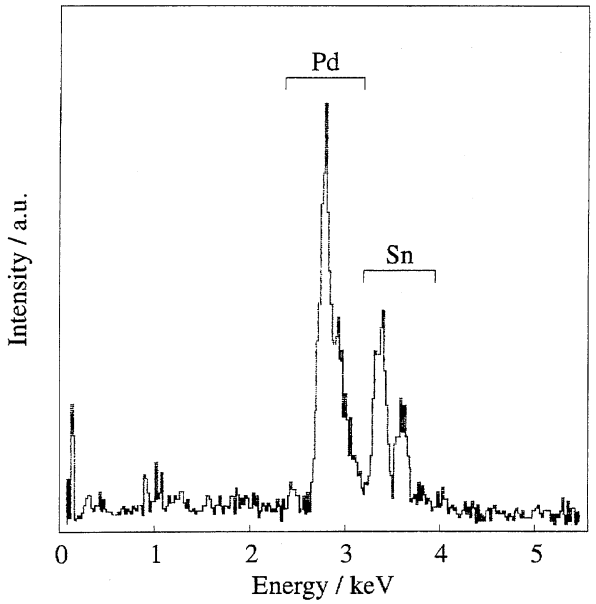

Fig. 3. EDX spectrum of 1 wt% Pd/SnO_2.

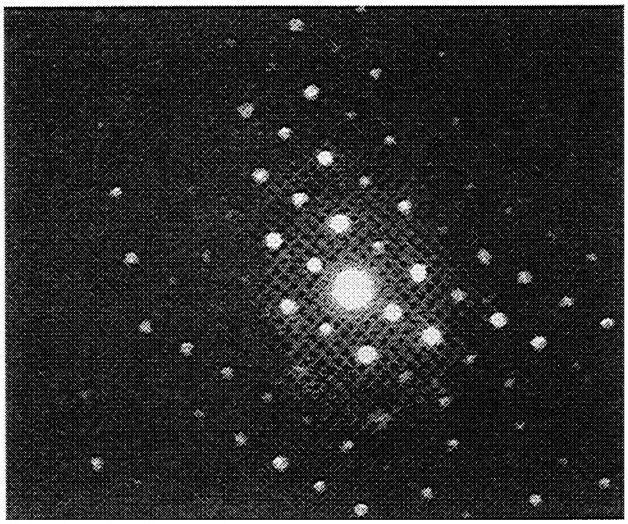

Fig. 4. Microbeam diffraction pattern of 1 wt% Pd/SnO_2.

characteristic feature of Pd/SnO_2 is shown in Fig. 5. It is noted that the shell and core structures could be obviously seen in the high-resolution image. An amorphous-like PdO layer is uniformly formed as the outer shell of the particle, whereas the core region is well-crystallized SnO_2. Most of the particles with different size equally possessed such a microstructure under this condition. This microstructure is obviously different from that of Pd/Al_2O_3, as reported previously, in which only finely dispersed grains of palladium are deposited on the support oxide.[9]

3. TPD Experiment. To evaluate the correlations between the catalytic activity and the reduction-oxidation property of supported Pd, TPD experiments were performed. Figure 6 shows the TPD profiles of oxygen from bulk palladium without any support. It features a sharp oxygen release centered at ca. 680 °C. This desorption, being similar to that

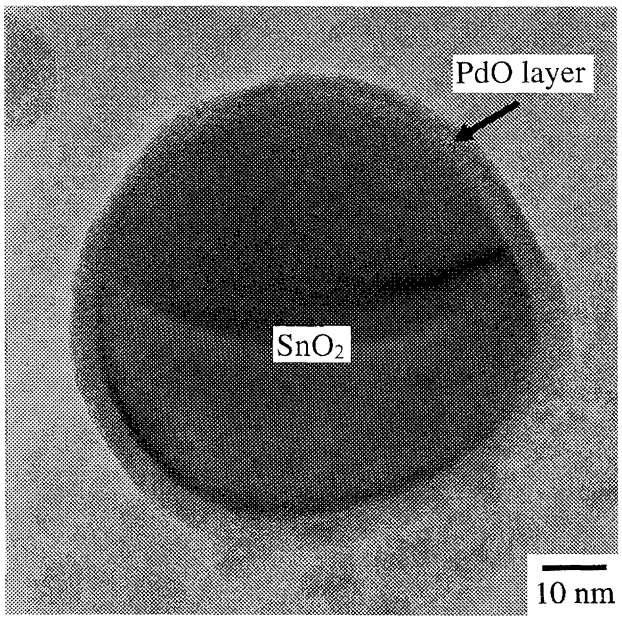

Fig. 5. High resolution TEM photograph of fine particles of 1 wt% Pd/SnO_2.

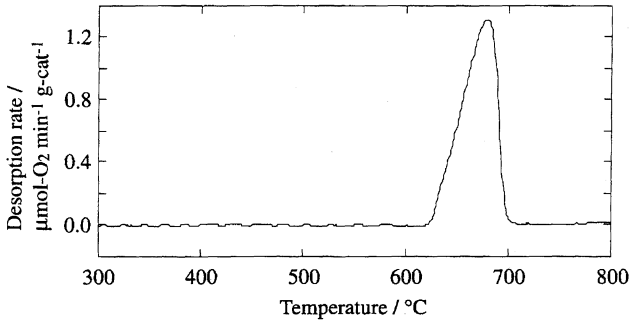

Fig. 6. TPD profile of oxygen from bulk Pd. Heating rate = 5 °C min^{-1}. Sample was heated O_2 stream at 800 °C for 2 h and subsequently cooled to room temperature prior to the measurement.

observed by Bell et al., is attributed to the oxygen dissociation of PdO bulk.[23] The PdO phase becomes thermodynamically unstable around this temperature; thus, the peak accompanies the decomposition of the bulk oxide into metallic Pd.

The TPD curves of oxygen from the Al_2O_3, Al_2O_3–36NiO, and SnO_2 support without palladium are illustrated as bold lines in Fig. 7. No desorption of oxygen was detected from the Al_2O_3 and Al_2O_3–36NiO supports, while the SnO_2 support indicated small and broad desorption of oxygen at ca. 430 °C. The TPD curves of oxygen from the supported Pd catalysts (Pd/Al_2O_3, Pd/Al_2O_3–36NiO, and Pd/SnO_2) are

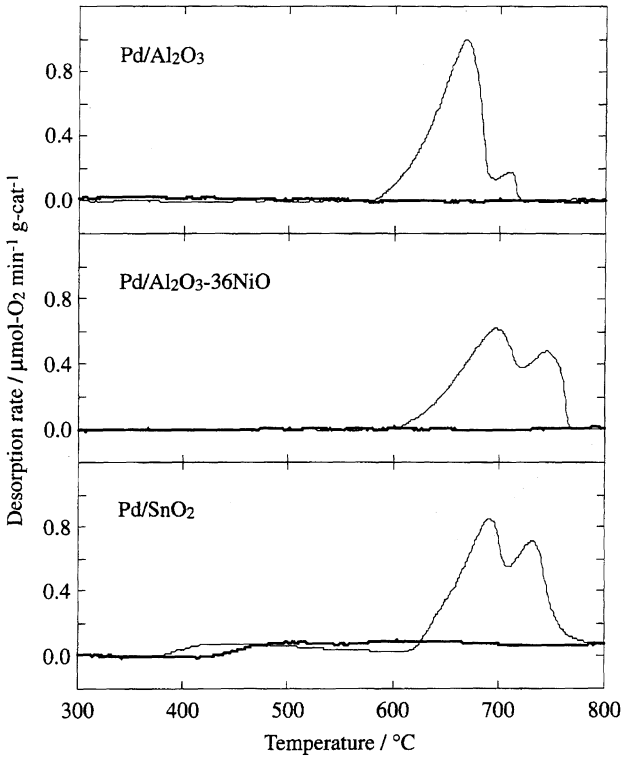

Fig. 7. TPD profiles of oxygen from 1 wt% Pd/Al_2O_3, 1 wt% Pd/Al_2O_3–36NiO, 1 wt% Pd/SnO_2, and from the support oxides. Heating rate = 5 °C min^{-1}. Sample was heated in O_2 stream at 800 °C for 2 h and subsequently cooled to room temperature prior to the measurement.
— supported Pd catalyst, — support oxide.

also shown in Fig. 7 as fine solid lines. It is revealed that the TPD profiles of oxygen from the three kinds of supported palladium considerably differ from the single desorption peak from bulk palladium without supports (Fig. 6). For the supported Pd samples, oxygen desorption in the temperature range of 600—750 °C splits into two peaks. For Pd/Al_2O_3, two distinct peaks were observed at ca. 660 and 720 °C. Therefore, these peaks reflect the different adsorption states of oxygen on palladium. It can be clearly seen that the relative ratio of the low- and high-temperature desorption peaks depends on the kind of support. A large high-temperature peak appeared for the Pd/Al_2O_3–36NiO and Pd/SnO_2 catalysts. The shapes and temperatures of the TPD curves for Pd/SnO_2 and Pd/Al_2O_3–36NiO are quite similar to each other, correlating well with their similar catalytic activities. However, in the case of Pd/SnO_2, oxygen desorption was also observed at ca. 400—600 °C, while the Pd/Al_2O_3–36NiO catalyst did not exhibit desorption in this temperature range. The broad peak observed at low temperatures should be attributed to oxygen released from the SnO_2 support.

4. XPS Experiment. The relations between the catalytic activity and the electronic state of supported Pd was investigated by XPS experiments. Verduraz et al. have reported a strong metal-oxide interaction for Pd.[24] Figure 8 shows the XPS profiles of Pd 3d from fresh samples after heating in air at 800 °C. Another spectrum was recorded for each sample after a reduction treatment at room temperature. A fresh sample after an XPS measurement was exposed to a hydrogen-nitrogen mixture in a pretreatment chamber installed on the XPS apparatus. The vertical lines displayed in the figures are the Pd $3d_{5/2}$ binding energies observed for metallic palladium at 335.9 eV and PdO at 337.6 eV for the Pd/Al_2O_3 sample.

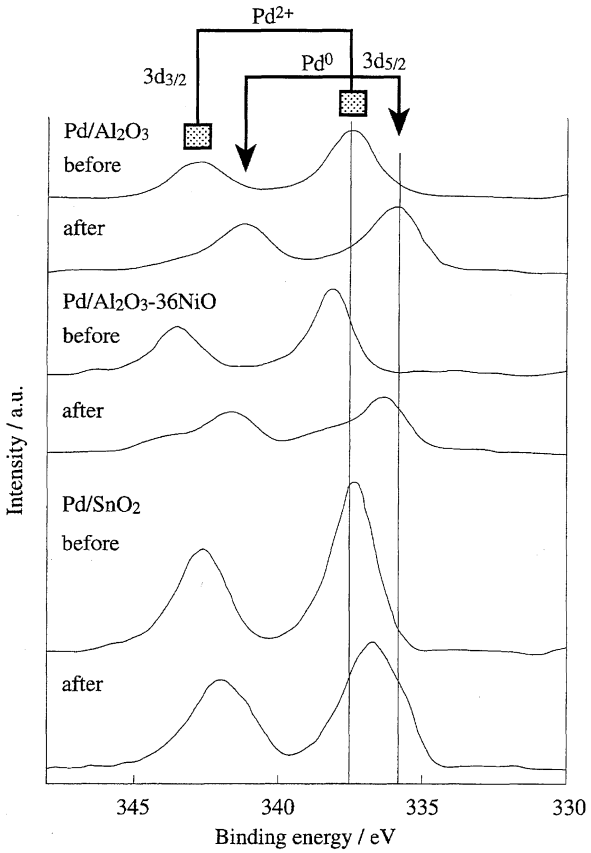

Fig. 8. Pd 3d X-ray photoelectron of 1 wt% Pd/Al_2O_3, 1 wt% Pd/Al_2O_3–36NiO, and 1 wt% Pd/SnO_2 before and after H_2 reduction at room temperature.

The Pd $3d_{5/2}$ line of every supported Pd sample after heating in air is attributed to a single peak from the oxide, reflecting the complete oxidation of palladium. However, the peak center was shifted to a higher binding energy for Pd/Al_2O_3–36NiO and Pd/SnO_2 than for Pd/Al_2O_3. The spectrum for Pd/Al_2O_3 was shifted to a lower binding energy to form a single peak centered at 335.9 eV after reduction at room temperature. The surface of the palladium particles was completely reduced to the metallic state, even at room temperature. In the case of Pd/Al_2O_3–36NiO, the shift of Pd spectrum from PdO to Pd metal was also observed; however the PdO state still overlapped to some extent. It should be noted that the Pd spectrum of Pd/SnO_2 was broadened after reduction at room temperature, whereas neither peak splitting nor a peak shift was obvious. From a computer peak-fit, the spectrum was shown to consist of two sets of Pd $3d_{5/2}$ lines at 337.5 and 335.8 eV from different oxidation states, though the extent of the reduction of palladium on the Pd/SnO_2 sample was smaller than the other two samples.

5. In situ XRD Experiment. From the TPD experiments mentioned in the previous section, it is shown that the adsorption state of oxygen on palladium is strongly affected by the support. The use of SnO_2 or Al_2O_3–36NiO allows palladium particles to exist in a higher oxidation state than on Al_2O_3. The stability of the PdO phase in these catalysts was measured by in situ X-ray diffraction. As we have already reported previously, the diffraction line of Pd (111) was used for estimating the stability of the PdO phase.[9] The relative intensities of the metallic Pd (111) diffraction line of Pd/Al_2O_3, Pd/Al_2O_3–36NiO, and Pd/SnO_2 samples are plotted as a function of the temperature in Fig. 9. The intensity at some temperature (T) is referenced with those after complete decomposition of palladium to the metallic state at 800 °C for Pd/Al_2O_3 and at 860 °C for Pd/Al_2O_3–36NiO and Pd/SnO_2. The thermal decomposition of PdO on Al_2O_3 started at 710 °C and completed at 800 °C. For Pd/Al_2O_3–36NiO and Pd/SnO_2 catalysts, the PdO phase was more stable than for Pd/Al_2O_3, and the dissociation of oxygen proceeded at higher temperatures. It is revealed that the change in the palladium phase of Pd/SnO_2 observed by the in situ XRD method is similar to that of Pd/Al_2O_3–36NiO, reflecting the same tendency as their TPD and XPS results.

Discussion

The activity for methane oxidation over palladium strongly depends on the support material, as indicated in Fig. 1. The Pd/SnO_2 catalyst shows the most excellent activity. It was not possible to gain the activity of Pd/SnO_2 by mixing with other metal oxides. However, it is interesting to note that, despite its low surface area, Pd/SnO_2 shows a higher cat-

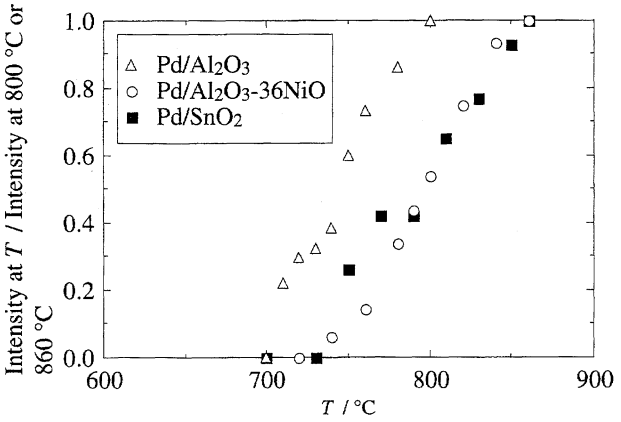

Fig. 9. Relative peak intensity of Pd (111) diffraction line of 1 wt% Pd/Al_2O_3, 1 wt%Pd/Al_2O_3–36NiO, and 1 wt% Pd/SnO_2 catalysts at various temperatures (T).

alytic activity than that of Pd/Al_2O_3 (Table 2). It has been known that tin dioxide is one of the active oxide catalysts for alkene oxidation.[25] This behavior has been explained based on cooperation between the oxides in oxygen adsorption through the so-called "remote control effect", as a result of the spillover of oxygen atoms from the donor phase to SnO_2.[26,27] The palladium–tin(IV) oxide system is popularly used for gas-sensing devices[28] and as a catalytic activator in CO oxidation.[14—16] The synergistic effect which is responsible for the enhanced catalytic activity by CO spillover has also been reported to be a unique catalytic property of Pd/SnO_2. Generally, the rate of reoxidation of palladium is faster for small particles than for large particles.[8,10,22,29] The particle size of palladium is affected by the interaction with oxides. The PdO crystallite size, evaluated by the X-ray line broadening method, indicated that palladium(II) oxide (PdO) is more finely dispersed on Al_2O_3–36NiO than on Al_2O_3.[17] The fine PdO crystallites on Al_2O_3–36NiO led to a high catalytic activity, as compared with Pd/Al_2O_3. It can be inferred that the particle size of PdO is an important factor for enhancing the catalytic activity. The PdO particle is also expected to be highly dispersed on SnO_2, as in the case of Pd/Al_2O_3–36NiO, judging from its similar catalytic property. Unlike the Pd/mAl_2O_3–nNiO catalyst,[17] an evaluation of the PdO particle size from the half width at the half maximum (HWHM) by the X-ray line-broadening method was impossible in the case of Pd/SnO_2, due to a strong overlap of the SnO_2 (101) line with the weak PdO (101) line.

The morphology of palladium particles dispersed on a SnO_2 support was observed by TEM. Although large particles substantially existed in a Pd/SnO_2 sample, the number of fine particles can also be seen in Fig. 2. It is revealed from the high-resolution image and EDX measurement of the fine particles that palladium(II) oxide was dispersed on SnO_2 supports by eventually forming an egg-shell-shaped layer. This microstructure implies a strong chemical interaction between PdO and SnO_2. The egg-shell-shaped microstructure appears to be unstable at high temperatures. Even if the layered structure of PdO is destroyed by sintering, fine palladium particles are expected to exist on the SnO_2 support. The sintering of PdO should be slower on SnO_2 than on a support without any chemical interaction. The high activity of the Pd/SnO_2 catalyst is originated from the effective surface exposure of active Pd surfaces on the support oxide.

From the Al_2O_3 and Al_2O_3–36NiO support oxides, oxygen did not desorb at or below 600 °C during a TPD measurement. However, the SnO_2 support, itself, showed oxygen desorption (Fig. 7). Such broad oxygen desorption from the SnO_2 support was also observed for the Pd/SnO_2 catalyst in the same temperature range.[30] Considering the similar catalytic behavior of Pd/SnO_2 and Pd/Al_2O_3–36NiO, the oxygen species attributed to the SnO_2 support is not directly involved in the reaction. The overall oxidation of Pd/SnO_2 is predominantly determined by the oxygen species on Pd.

The desorption curves of oxygen from the active Pd catalysts are characterized by two oxygen species which desorb at higher temperatures than less active catalysts; especially, the active catalysts always exhibited large desorption of the second peak. Many studies have shown that TPD profiles of oxygen are sensitive to the kind of support materials and the dispersion of palladium.[31] Thus, even for catalysts with the same weight loading of palladium, significant differences are observed in the TPD curves of oxygen from Pd on different supports. A comparison of the TPD profiles of supported Pd (Fig. 7) to that of unsupported bulk Pd (Fig. 6) indicates that oxygen desorption associated with the first peak at about 660—680 °C is from bulk PdO in the supported palladium catalysts. The peak observed at about 720 °C can be attributed to a stable oxide species (PdO_x), as has been suggested by McCarty.[32] Thus, it may be inferred that the second peak is attributable to oxygen desorption from Pd under a strong support interaction. Liske and Volter also observed two palladium oxide species on Pd/Al_2O_3, having different reducibility with hydrogen.[29] The bulk PdO phase is easily reducible, but the oxide is stabilized by the strong interaction with the alumina support to form a two-dimensional surface complex. Since the amount of desorption of the second peak is large due to Pd/Al_2O_3–36NiO or Pd/SnO_2, the Pd-support interaction is not merely ascribed to the triple phase boundary of Pd-support-gas phase or in the vicinity of the boundary. The influence of the supports may extend to at least several layers of palladium atoms from the contacting interface. It can be considered that the support effects observed as the second peak for Pd/Al_2O_3–NiO and Pd/SnO_2 is very important in determining the catalytic activity.

To elucidate the relation between the catalytic activity and chemical state of Pd, an XPS measurement was then employed. An obvious difference in the chemical state was observed in the reducibility of palladium, though the original binding energies of palladium were only slightly different for the examined samples. From Fig. 8, Pd/Al_2O_3 is reduced almost completely to the metallic state upon exposure to hydrogen at room temperature. After the same reduction treatment, the oxidized form of palladium was retained for Pd/Al_2O_3–36NiO and Pd/SnO_2. Otto et al. reported that oxidized palladium supported on γ-Al_2O_3 at loadings greater than 0.5 wt% exists as PdO bulk, which is completely re-

duced to metallic palladium at 25 °C, whereas at loadings below this level, palladium species existed as a more highly dispersed state.[33] Thus, the interaction with the support stabilizes the oxidized state, i.e., the Pd species are reduced at higher temperatures. The XPS results suggest that the strong Pd-support interaction stabilizes the high oxidation state of Pd.

An in situ XRD measurement also confirmed the high stability of the PdO phase on SnO_2 and Al_2O_3–36NiO supports, as compared with Al_2O_3 (Fig. 9). Thus, three characterization procedures equally suggest that high oxidation state palladium is stabilized on SnO_2 and Al_2O_3–36NiO. In general, palladium oxide is the more active for methane combustion than the metallic form; namely, significant deactivation is accompanied by the decomposition of the oxide to metallic palladium. A strong correlation between the stability of the PdO phase and the catalytic activity indicates that the PdO-support interaction is an important factor for enhancing the catalytic activity.

From these results, it can be inferred that the origin of the support effect is twofold. The palladium layer dispersed on the support in an egg-shell structure provides a large palladium surface active for the catalytics reaction as the result of an intimate contact between Pd and a tin(IV) oxide support. Although an egg-shell type layered structure was not observed for Pd/Al_2O_3–36NiO, this support is also expected to be effective to maintain the high dispersion state of PdO. The second support effect appears as an interaction between Pd and oxygen. The supports also influence the Pd–oxygen bond; i.e., the stability of the high oxidation state of Pd on SnO_2 or Al_2O_3–36NiO is directly related with the oxidation catalysis.

Conclusion

Pd catalysts supported on metal oxides, especially SnO_2-based oxides, were investigated for developing catalyst materials for the ignition of methane. Alumina is generally used as a conventional support for Pd catalysts for methane combustion. The Pd catalyst supported on SnO_2 was found to have excellent activity for the complete oxidation of methane, although the BET surface area of the SnO_2 support was far smaller than that of Al_2O_3. From a TEM observation, palladium oxide was observed as a surface layer which uniformly covers SnO_2 fine particles by forming an egg-shell structure. This initial microstructure results in the large active surface of palladium. The change in the chemical properties, especially the redox property of palladium, was significantly affected by the kind of support. Methane combustion was found to be dependent on the oxygen adsorption state on palladium, as revealed from the TPD results. A strong similarity could be found in the TPD curve from the active catalysts for CH_4 combustion. The reducibility properties of palladium measured by XPS method was also significantly affected by the kind of support. The use of SnO_2 as a support can suppress the dissociation of PdO at higher temperatures. Methane combustion was found to be dependent on the dispersion and oxidation states of palladium through an interaction with the support. The high catalytic activity of Pd/SnO_2 offers an interesting perspective concerning methane combustion for various applications.

References

1) D. L. Trimm, *Appl. Catal.*, **7**, 249 (1983).
2) R. Prasad, L.A. Kennedy, and E. Ruckenstein, *Catal. Rev.*, **26**, 1 (1984).
3) H. Sadamori, T. Tanioka, and T. Matsuhisa, *Proc. Int. Workshop Catal. Combust.*, **2**, 158 (1994).
4) R. F. Hicks, H. Qi, M. L. Young, and R. G. Lee, *J. Catal.*, **122**, 280 (1990).
5) P. Briot and M. Primet, *Appl. Catal.*, **68**, 301 (1991).
6) E. Garbowski, C. Feumi-Jantou, N. Mouaddib, and M. Primet, *Appl. Catal. A*, **109**, 277 (1994).
7) F. H. Ribeiro, M. Chow, and R. A. Dalla Betta, *J. Catal.*, **146**, 537 (1994).
8) C. F. Cullis and B. M. Willatt, *J. Catal.*, **83**, 267 (1983).
9) H. Widjaja, K. Sekizawa, K. Eguchi, and H. Arai, *Catal. Today*, in press.
10) T. R. Baldwin and R. Burch, *Appl. Catal.*, **66**, 359 (1990).
11) J. G. E. Cohn and A. J. Haley, *Can. Pat.*, **597**, 459 (1960).
12) R. Burch, F. J. Urbano, and P. K. Loader, *Appl. Catal. A*, **123**, 173 (1995).
13) R. J. Cvetanovic and Y. Amenomiya, *Adv. Catal.*, **17**, 103 (1967)
14) E. R. S. Winter, *Adv. Catal.*, **10**, 196 (1958).
15) M. Sheintuch, J. Schmidt, Y. Lechtman, and G. Yahav, *Appl. Catal.*, **49**, 55 (1989).
16) D. R. Schryer, B. T. Upchurch, J. D. Van Norman, K. G. Brown, and J. Schryer, *J. Catal.*, **122**, 193 (1990).
17) H. Widjaja, K. Sekizawa, K. Eguchi, and H. Arai, *Catal. Today*, **35**, 197 (1997).
18) R. J. Farrauto, M. C. Hobson, T. Kennelly, and E. M. Waterman, *Appl. Catal. A*, **81**, 227 (1992).
19) P. Salomonsson, S. Johansson, and B. Kasemo, *Catal. Lett.*, **33**, 1 (1995).
20) C. A. Muller, R. A. Koeppel, M. Maciejewski, and A. Baiker, *Appl. Catal. A*, **145**, 335 (1996).
21) R. J. Farrauto, J. K. Lampert, M. C. Hobson, and E. M. Waterman, *Appl. Catal.*, **6**, 263 (1995).
22) T. R. Baldwin and R. Burch, *Appl. Catal.*, **66**, 337 (1990).
23) W. E. Bell, R. E. Inyard, and M. Tagami, *J. Phys. Chem.*, **70**, 3735 (1966).
24) F. B. Verduraz, A. Omar, J. Escard, and B. Pontvianne, *J. Catal.*, **53**, 126 (1978).
25) F. S. Berry, *Adv. Catal.*, **30**, 97 (1981).
26) L. T. Weng and B. Delmon, *Appl. Catal. A*, **81**, 141 (1992).
27) L. T. Weng, N. Spitaels, B. Yasse, J. Coudriere, P. Ruiz, and B. Delmon, *J. Catal.*, **132**, 319 (1991).
28) T. Seiyama, H. Futata, F. Era, and N. Yamazoe, *Denki Kagaku*, **40**, 244 (1972).
29) H. Lieske and J. Volter, *J. Phys. Chem.*, **89**, 1841 (1985).
30) N. Yamazoe, J. Fuchigami, M. Kishikawa, and T. Seiyama, *Surf. Sci.*, **86**, 335 (1979).
31) T. E. Hoost and K. Otto, *Appl. Catal. A*, **92**, 39 (1992).
32) J. G. McCarty, *Catal. Today*, **26**, 283 (1995).
33) K. Otto, L. P. Haack, and J. E. deVries, *Appl. Catal. B*, **1**, 1 (1992).